Facile Synthesis, Characterization, and Microwave Absorbability of CoO Nanobelts and Submicrometer Spheres

ARTICLE *in* THE JOURNAL OF PHYSICAL CHEMISTRY C · APRIL 2009

Impact Factor: 4.77 · DOI: 10.1021/jp8092447

5 AUTHORS, INCLUDING:

Genban Sun
Beijing Normal University
33 PUBLICATIONS **1,039** CITATIONS
SEE PROFILE

Xiaoqiang Zhang
University of Victoria
2 PUBLICATIONS **74** CITATIONS
SEE PROFILE

Minhua Cao
Beijing Institute of Technology
129 PUBLICATIONS **4,035** CITATIONS
SEE PROFILE

Bingqing Wei
University of Delaware
251 PUBLICATIONS **12,275** CITATIONS
SEE PROFILE

THE JOURNAL OF PHYSICAL CHEMISTRY C

Article

Facile Synthesis, Characterization, and Microwave Absorbability of CoO Nanobelts and Submicrometer Spheres

Genban Sun, Xiaoqiang Zhang, Minhua Cao, Bingqing Wei, and Changwen Hu

J. Phys. Chem. C, **2009**, 113 (17), 6948-6954• DOI: 10.1021/jp8092447 • Publication Date (Web): 03 April 2009

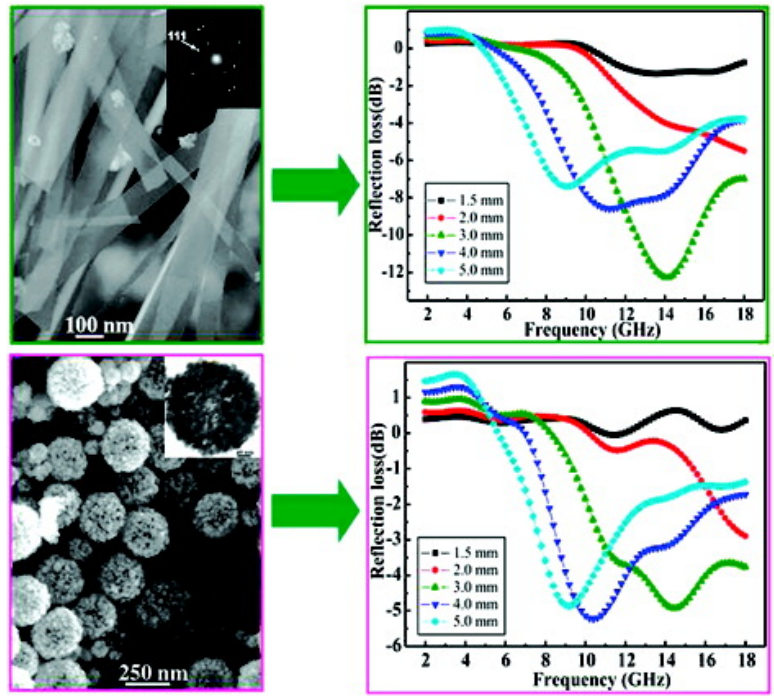

More About This Article

Additional resources and features associated with this article are available within the HTML version:

- Supporting Information
- Access to high resolution figures
- Links to articles and content related to this article
- Copyright permission to reproduce figures and/or text from this article

View the Full Text HTML

The Journal of Physical Chemistry C is published by the American Chemical Society. 1155 Sixteenth Street N.W., Washington, DC 20036

Facile Synthesis, Characterization, and Microwave Absorbability of CoO Nanobelts and Submicrometer Spheres

Genban Sun,*,† Xiaoqiang Zhang,† Minhua Cao,‡ Bingqing Wei,*,§ and Changwen Hu‡

College of Chemistry, Beijing Normal University, Beijing, 100875, People's Republic of China, The Institute for Chemical Physics and Department of Chemistry, Beijing Institute of Technology, Beijing 100081, People's Republic of China, and Department of Mechanical Engineering, University of Delaware, Newark, Delaware 19716

Received: October 19, 2008; Revised Manuscript Received: March 13, 2009

Single crystal CoO nanobelts with thicknesses of several nanometers and widths of 30−100 nm and polycrystalline CoO submicrometer spheres self-assembled by nanoparticles with diameters ranging from 20 to 40 nm were synthesized via a microemulsion method under solvothermal conditions. The shape and size of CoO nanostuctures can be well controlled by H_2O/surfactant molar ratio and other solvothermal parameters. Apart from structural and morpholoical characterizations of the submicrometer spheres and the nanobelts, powder X-ray diffraction, electron microscopy techniques, and microwave absorption properties of typical samples have also been investigated. The results indicate that the microwave absorption of nanobelts is stronger than that of submicrometer spheres.

Introduction

The synthesis of low dimensional transition metal oxide nanostructures, for example, zero-dimensional (0D) nanocrystals, one-dimensional (1D) nanotubes, nanowires, and nanobelts, and three-dimensional (3D) submicrometer spheres have been a research theme for decades as driven by their chemical stability and widespread use in magnetic data storage, battery materials, catalysts, sensors, and ferrofluids.[1] In particular, cobalt monoxide (CoO) 1D nanobelts, and 3D submicrometer spheres, crystallizing in rock salt structure, are significant owing to their potential applications based on electric, magnetic, catalytic, and gas-sensing properties.[2] In recent years, several research groups have successfully reported the synthesis of CoO 0D nanocrystals via different methods, respectively.[3] In addition, An et al. synthesized pencil-shaped CoO nanorods by the thermal decomposition of a cobalt−oleate complex.[4] Peng's research group have successfully reported CoO nanoflowers grown by limited ligand protection.[5] Xu et al. prepared CoO nanosheets by the reducing agent $NaBH_4$ via an ultrasonication method.[6] Very recently, Zhang et al. reported a series of cubic CoO 0D nanocrystals with various morphologies and sizes via the decomposition of cobalt(II) oleate complex in noncoordinating solvent octadecene containing dodecanol/oleic acid.[7] But to the best of our knowledge, no method has been reported for the synthesis of CoO 1D nanobelts and 3D submicrometer spheres. Therefore, controlled synthesis of CoO 1D and 3D nanostructures is still a challenging task due to their unique properties. The microemulsion-mediated solvothermal method has been widely used to synthesize nanoscale materials because of its several advantages, resulting from its unique reaction environment.[8] In this paper, we demonstrate that very stable CoO nanobelts and submicrometer spheres with a cubic rock salt structure can be synthesized by a microemulsion system, cetyltrimethylammonium bromide (CTAB)/water/cyclohexane/1-pentanol. The size and shape of CoO nanostructures can be readily tuned by adjusting experimental parameters of the microemulsion system. In addition, the microwave absorption performance of CoO nanobelts and submicrometer spheres were discussed in detail.

Experimental Section

Synthesis. All the reagents were of analytical purity and used without further purification. CTAB, cyclohexane, 1-pentanol, K_2CO_3, and $KHCO_3$ were purchased from Beijing Chemical Reagent Limited Corporation. $NH_3 \cdot H_2O$ were purchased from Beijing Yili Fine Chemicals Limited Corporation. $Cu(NO_3)_2 \cdot 6H_2O$ was purchased from Shanghai Chemical Reagents Limited Corporation, and the cobalt precursor $[Co(NH_3)_6]Cl_3$ was synthesized according to the method reported by Kruger et al.[9]

As a typical synthesis, two identical solutions were first prepared by dissolving CTAB (2 g) in 50 mL of cyclohexane and 2 mL of 1-pentanol. The mixed solution was stirred for at least 30 min until it became transparent. Second, 0.4 g of $[Co(NH_3)_6]Cl_3$ was dissolved in water (8 mL), and the solution thus formed was added to one of the two microemulsions prepared in the first step with stirring. Third, 10 mL of an aqueous saturated solution of $K_2CO_3/KHCO_3$ (2.4 and 1.25 M, respectively) with a small amount of $Cu(NO_3)_2 \cdot 6H_2O$ (ca. 0.1 g) was added to the other microemulsion under stirring. After the mixtures were substantially stirred, the two optically transparent microemulsion solutions were mixed and formed a glaucous suspending solution which was then transferred into an 80 mL Teflon-lined autoclave and heated at 180 °C for 12 h. The resulting suspension was allowed to cool naturally down to room temperature. The precipitate and blue remanent solution of $[Cu(NH_3)_4]^{2+}$ could be separated after centrifugation. Then the precipitate was washed several times with absolute ethanol and distilled water and dried in vacuum at 40 °C for 12 h. Brown nanostructured materials of CoO were obtained. Note that the

* Corresponding authors, gbsun@bnu.edu.cn (G. Sun) and weib@udel.edu (B. Wei).
† Beijing Normal University.
‡ Beijing Institute of Technology.
§ University of Delaware.

10.1021/jp8092447 CCC: $40.75
Published on Web 04/03/2009

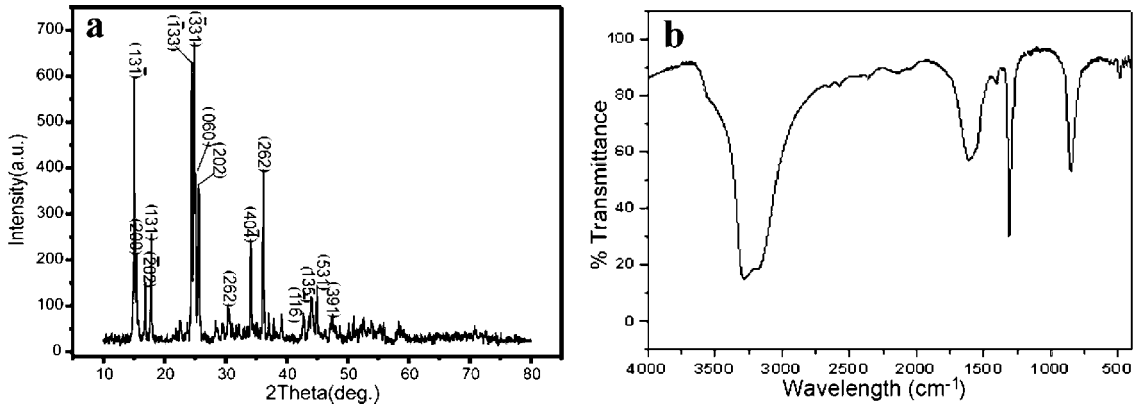

Figure 1. (a) XRD and (b) FTIR of the precursor material $Co(NH_3)_6Cl_3$.

molar ratio of CTAB and water (defined as *w*) is about 40 in sphere preparation. while the CoO nanobelts were prepared at $w = 20$.

Characterization. The composition and phase purity of the as-synthesized samples were analyzed by X-ray diffraction (XRD) patterns obtained with a SHIMADZU XRD-6000 operated at 40 kV voltage and 50 mA current with Cu Kα radiation ($\lambda = 1.5418$ Å). Field emission scanning electron microscopy (FE-SEM) images and energy dispersive X-ray (EDX) spectra were obtained on a field emission microscope (XL30 S-FEG, FEI) operated at an acceleration voltage of 10 kV and an EDX instrument (EDAX NEW XL-30, America). The X-ray photoelectron spectra (XPS) of the nanostructures were recorded with a PHI Quantera SXM Instrument using a monochromatized Al Kα source after sputtering the samples to different depths with an Ar^+ ion beam at 2.0 keV. The resolution of the spectrum reported here is approximately 0.5 eV. The binding energy of the samples was calibrated by setting the C 1s peak to 284.8 eV. Transmission electron microscopy (TEM) and high-resolution TEM (HRTEM) images were obtained on a JEOL JEM-2010 transmission electron microscope at an acceleration voltage of 200 kV. Fourier transform IR (FT-IR) spectra were recorded on a Nicolet MAGNA-IR 560 spectrometer with a wide-band MCT liquid-nitrogen-cooled detector and a KBr beam splitter. CoO nanostructures/paraffin composite samples were prepared by uniformly mixing the nanostrucutres in a paraffin matrix and then pressing the mixture into a cylindrical-shaped compact ($\Phi_{outer} = 7.00$ mm and $\Phi_{inner} = 3.04$ mm). The electromagnetic (EM) parameters of the nanostructures composites with 70 wt % of CoO nanostructures were measured in a 2−18 GHz range by using an Agilent E8362B vector network analyzer.

Results and Discussion

To indicate the molecular formula of the precursor material we prepared, XRD pattern and FTIR spectra were employed. From the XRD pattern (Figure 1a), all of the diffraction peaks can be indexed to monoclinic phase with end-centered structure (ICDD JCPDS card: 700787), which confirms that the precursor material $[Co(NH_3)_6]Cl_3$ demonstrates a good crystallinity and no other impurities were detected. The FT-IR spectra of the precursor material are shown in Figure 1b. The spectral peaks provide vibrational information for the functional groups in the samples, which is very important for characterizing the structure and composition of the material. From Figure 1b, as reported before,[10] we conclude that $[Co(NH_3)_6]Cl_3$ has four characteristic peaks: the stretching vibration of NH_3 and O−H in the crystallization water (appearing at 3400−3000 cm^{-1}), the degenerate distortion (1650−1550 cm^{-1}), symmetric distortion (1370−1000 cm^{-1}), and rocking vibration (950−590 cm^{-1}).

The XRD patterns of the CoO nanobelts and submicrometer spheres obtained under solvothermal temperature (*T*) of 180 °C with *w* values of 20 and 40 are provided in Figure 2, which clearly show pure crystalline and cubic phases. The diffraction peaks of the cubic phase (patterns a and b in Figure 2) are well matched with those of the corresponding bulk CoO congener (*Fm*3*m*, $a = 4.26$ Å, JCPDS No. 48-1719). It was found that peaks (111) of patterns a and b in Figure 2 are the only peaks that gain a substantial increase in relative intensity, indicating that the nanostructures growth may occur along the [111] direction. As given in patterns c and d of Figure 2, when $T =$ 140 °C, there are some Co_3O_4 nanoparticles coexisting with CoO nanostructures. The diffraction patterns with asterisks are derived from Co_3O_4 nanocrystals. We speculated that the autogenous pressure generated in the sealed autoclave allowed the temperature to go higher than the boiling point of the solvent and the existence of the reductant such as 1-pentanol and NH_3. Higher temperature can make the conversion of Co_3O_4 impurity to CoO, completely, according to the reaction $Co_3O_4 \rightarrow 3CoO + {}^1/_2O_2(g)$.[3e,11] In order to further confirm the elements of the nanostuctures, the EDX for nanobelts and submicrometer spheres obtained under $T = 180$ °C and $w = 20$ and 40 are shown in spectra e and f of Figure 2. From spectra e and f of Figure 2, we can conclude that the nanobelts and submicrometer spheres only consist of the elements of Co and O, and the C element is ascribed to the rubberized fabric which is used for pasting in the sample. Moreover, to better assess the chemical nature of the nanostructures prepared in the present study, XPS were also employed. The XPS spectra of the as synthesized CoO nanobelts and submicrometer spheres are shown in Figure 3. The peak at 780.0 eV is from Co $2p_{3/2}$,[12a] with a shakeup satellite at 789.1 eV,[12b] while the peak at 796.0 eV is caused by Co $2p_{1/2}$,[3g] with a satellite peak at 805.7 eV.[12b] The presence of those two highly intense peaks and the satellites near them is consistent with the presence of Co^{2+} in the high-spin state. The absence of a signal at 778.1 eV indicates the nonexistence of Co metal impurities.[3e] The EDX and XPS spectra of the as synthesized CoO nanostructures confirm that the nanospheres and nanobelts only consist of the elements of Co and O and the ratio of Co and O is about 1:1, which is well in agreement with the XRD data.

When a *w* value of 20 was employed, CoO nanobelts were obtained. Figures 4a, 4b and 6c show the SEM images of the nanobelts with different magnifications. Large scales of nanobelts with typical lengths in the range of several tens of micrometers, widths of 30−100 nm, and thicknessess of several

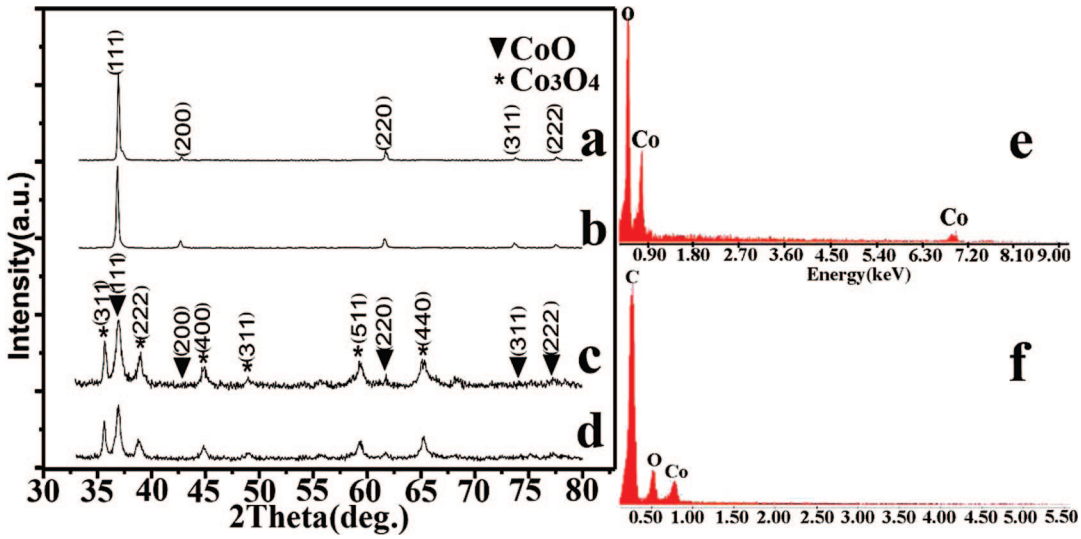

Figure 2. XRD patterns of the (a) nanobelts obtained at $w = 20$, $T = 180$ °C. (b) Nanospheres obtained at $w = 40$, $T = 180$ °C. (c) Nanobelts obtained at $w = 20$, $T = 140$ °C. (d) Nanospheres obtained at $w = 40$, $T = 140$ °C. EDX spectra of (e) CoO nanobelts and (f) CoO nanospheres.

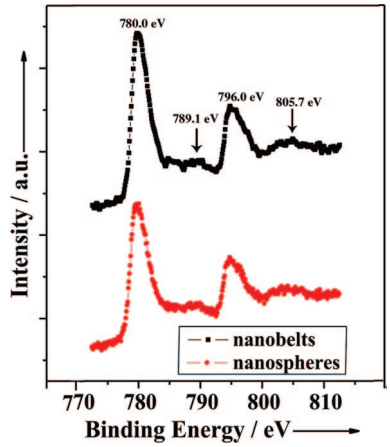

Figure 3. Co 2p XPS spectrum of CoO nanostructures at the energy range from 773 to 815 eV.

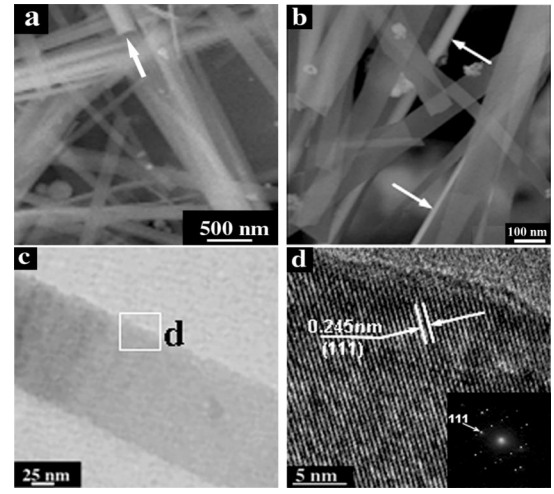

Figure 4. Electron microscopy characterization of CoO nanobelts obtained at $w = 20$, $T = 180$ °C. (a and b) SEM images of CoO nanobelts. (c) TEM image of a single nanobelt. (d) HRTEM image recorded in regions of the nanobelts labeled in (c). The inset of (d) is a photograph of the corresponding SAED pattern.

nanometers were observed. It is noteworthy that the nanobelts can be favoringly curled to thin nanowires along the vertical to axial direction under solvothermal conditions (See arrows in panels a and b of Figure 4). HRTEM images of the typical CoO nanobelt with the width of 100 nm are shown in panels c and d of Figure 4. It is evident that the HRTEM image in Figure 4d shows clear lattice fringes, indicating a single-crystalline nature of the entire beltlike structure. The lattice spacing of 2.45 Å between adjacent lattice planes corresponds to the distance between adjacent (111) crystal planes. The SAED pattern (inset of Figure 4d) taken from the same nanobelt clearly shows a single crystal structure and also indicates that the nanobelt is oriented along [111], which is consistent with the XRD pattern a given in Figure 2.

When the value of w was 40, sphere-shaped CoO nanostructures were formed. The SEM and low- and high-resolution TEM images of CoO nanospheres are illustrated in Figure 5 and Figure 6h. SEM observations showed that the product consists of a large quantity of spherical nanostructures with typical diameters in narrow range of 250−300 nm in Figure 5a. As shown in the higher-magnification SEM image in Figure 5b, the spheres are constructed of nanoparticles with diameters ranging from 20 to 40 nm. TEM image (inset of Figure 5b) clearly demonstrates a typical submicrometer sphere with a diameter of about 290 nm and the CoO nanocrystal building blocks with a diameter of 20 nm. In addition, it is speculated that the denseness of the nanocrystals at the edge of the submicrometer CoO spheres is thicker than the one at the center from Figure 5b, indicating a cagelike spherical structure. The HRTEM images taken from two different areas labeled c and d in Figure 5b clearly show the lattice image of the nanocrystals. As shown in panels c and d of Figure 5, the observed lattice spacing corresponding to the (111) lattice plane is estimated to be 2.45 Å and the one corresponding to the (220) lattice plane is estimated to be 1.51 Å, and the growth direction from the center to the edge of the nanocrystals is [111]. The SAED pattern (inset of Figure 5d) taken from the spheres shown in Figure 5b indicates that the CoO submicrometer spheres have polycrystalline structures, The strong diffraction rings were well indexed for the five characteristic faces of cubic CoO polycrystallines, which is consistent with the XRD pattern b given in Figure 2.

Figure 6 illustrates the size and shape evolution of the CoO nanostructures, which can be readily controlled by adjusting w. Figure 6b clearly shows the hollow spherical structure with

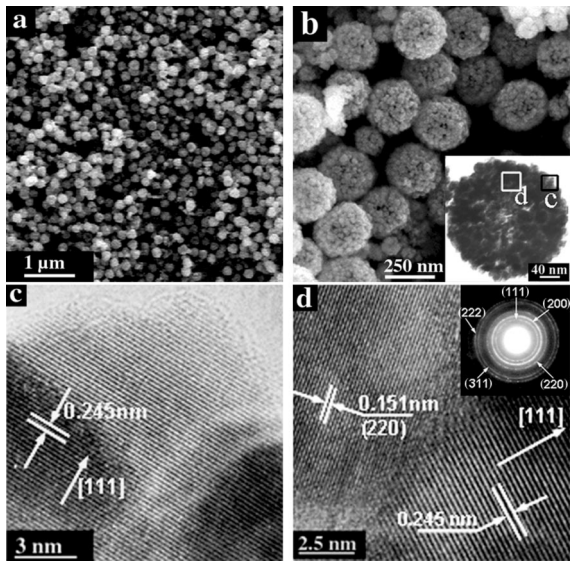

Figure 5. Electron microscopy characterization of CoO nanospheres obtained at $w = 40$, $T = 180$ °C. (a and b) SEM images of CoO nanospheres; the inset of (b) is a TEM image of a sphere structure. (c and d) High-resolution TEM images recorded in different regions of a single nanosphere labeled in the inset of (b). The inset of (d) is the corresponding SAED patterns.

a typical outer diameter of 90 nm and inner diameter of 50 nm when w was adjusted to 10. However, when $w = 25$, large scales of nanoparticles coexisting with nanobelts were observed (Figure 6d,e). When $w = 30$ or 50, there are large scales of nanoparticles coexisting with nanospheres. The nanospheres obtained under this condition have some defects of low-grade crystallization (Figure 6f,g and Figure 6i,j). As shown in panels f and g of Figure 6, the diameters of the spheres thus formed at $w = 30$ are ca. 150 nm, and the ones obtained at $w = 50$ are ca. 120 nm (Figure 6i,j). It is worth noting that the nanospheres in these two cases possess of a hollow structure (see Figure 6g,j). However with the absence of microemulsion, only nanoparticles about 30−40 nm were obtained (Figure 6k). As shown in Figure 5 and Figure 6h, only when $w = 40$ can CoO nanospheres with perfect morphologies be prepared. However, as shown in Figure 4 and Figure 6c−e, we concluded that the CoO nanobelts could be obtained with the condition of $w = 20$ or 25, but the nanobelts with perfect shapes could only be obtained with $w = 20$.

It has been reported that the size and shape of the nanostructures can also be tuned by adjusting the solvothermal time (t) and the solvothermal temperature (T).[8] Therefore, to explain the formation mechanism, different conditions which are important factors on the morphology were also explored such as t and T. The detailed results are included in Figures 7 and 8. Just as shown in Figure 7a, nanobelts coexisting with a few of nanoparticles can be obtained under the condition of $t = 1$ h and $w = 20$; the inset of Figure 7a more clearly indicates the nanobelts are bundle-like. But if $t = 6$ h, nanoparticles became fewer and more nanobelts with a long length of several micrometers were prepared (Figure 7b). From Figure 7b, we also concluded that there were no nanobelt bundles obtained under these conditions. For $w = 40$, the instance of nanospheres, if $t = 1$ h, a large number of nanospheres with a diameter of 120 nm were obtained (Figure 7c), and the inset of Figure 7c shows the nanospheres are assembled by many samll nanoparticles with sizes of about serveral nanometers. As shown in Figure 7d, when the solvothermal time was prolonged to 6 h, the nanospheres transformed into submicrometer spheres with porous structure, which were caused by the space between all of the bigger nanoparticles grown from the crystal nucleus. From Figure 8, when $T = 140$ °C and $w = 20$ and 40, products with different morphologies were observed. Figure 8a ($w = 20$) shows the morphology is a beltlike bundle, and very small nanoparticles (ca. 5−8 nm) were found on the surface of the nanobelts. The SAED pattern (inset of Figure 8a) indicates that the nanobelt bundles are polycrystalline. Figure 8b ($w = 40$) indicates large scales of spherelike morphology with diameters of 100−300 nm can also be obtained, but pure CoO cannot be prepared under the solvothermal temperature at 140 °C, these are the same peaks of Co_3O_4 indicated with asterisks in patterns c and d in Figure 2.

Although the reduction mechanism from Co^{3+} to CoO has not been clearly determined, 1-pentanol and NH_3 thus formed may act as the reductant in the reaction system. Moreover, a very small quantity of Cu^{2+} was necessary for synthesis of the cubic CoO nanostructures. With the absence of Cu^{2+}, only cubic Co_3O_4 nanoparticles instead of CoO nanostructures can be obtained. On the basis of the experiment results, we speculate that Cu^{2+} is to form the stable $[Cu(NH_3)_4]^{2+}$ and $[Cu(NH_3)_4]^{2+}$ cannot be decomposed under solvothermal conditions, which can be confirmed by the strong blue remanent solution. $[Co(NH_3)_6]^{3+}$ is forms an intermediate phase $Co_5(OH)_6(CO_3)_2$ and then is reduced and easily decomposed in synthesizing CoO nanostructures under solvothermal conditions. The role of Cu^{2+} should be studied in future experiments. Further research on the reaction mechanism is under way in our group. Though the reduction mechanism from Co^{3+} to CoO is not clear, we can propose the formation mechanism of the nanostructures as follows: The microemulsion plays an important role as a "soft" template in the formation of the CoO nanostructures. The molar ratio of H_2O to CTAB and the concentration of raw materials have a significant effect on the morphologies and sizes of the final products.[8] From the above experimental results, it can be inferred that the molar ratio of H_2O to CTAB (or the water content) as well as aggregation and coalescence of individual droplets are responsible for the formation of products with various morphologies. A schematic diagram of the proposed growth mechanism is shown in Figure 9. When two microemulsion solutions containing $[Co(NH_3)_6]^{3+}$ and $K_2CO_3/KHCO_3$ are mixed, CoO nucleation and irreversible micellar fusion may be coincident under an appropriate condition. When the w value is small, the low water content containing small exchangeable water molecules in the microemulsions may make the fuse rates between two spherical droplets very slow, which would result in a short cylinder droplet as shown in Figure 9. Such a microemulsion droplet comprises a centrally located beltlike CoO nucleus with water-enriched domains at the ends of the droplet. The surfactant molecules of side surfaces of the cylindrical droplet may adsorb on surface planes of the formed CoO nucleus, and therefore these surfactant molecules are fixed and immobile. In contrast, the surfactant molecules at both ends of the cylindrical droplet do not associate with CoO nucleus due to water-enriched domains at this field and are relatively free. Thus, the cylindrical microemulsion droplet may dynamically exchange with other microemulsions very fast at both ends of the droplet.[13] This process may result in the formation of CoO nanobelts. When higher water content (high value of w) was used, the formed microemulsion system might be low microviscosity and instability. Therefore, the fuse rate between two spherical droplets would be significantly increased, and so nearly spherical droplets with the CoO primary nucleus in the center of the spheroid were formed because of low surface energy and high stability. The water-enriched domains equili-

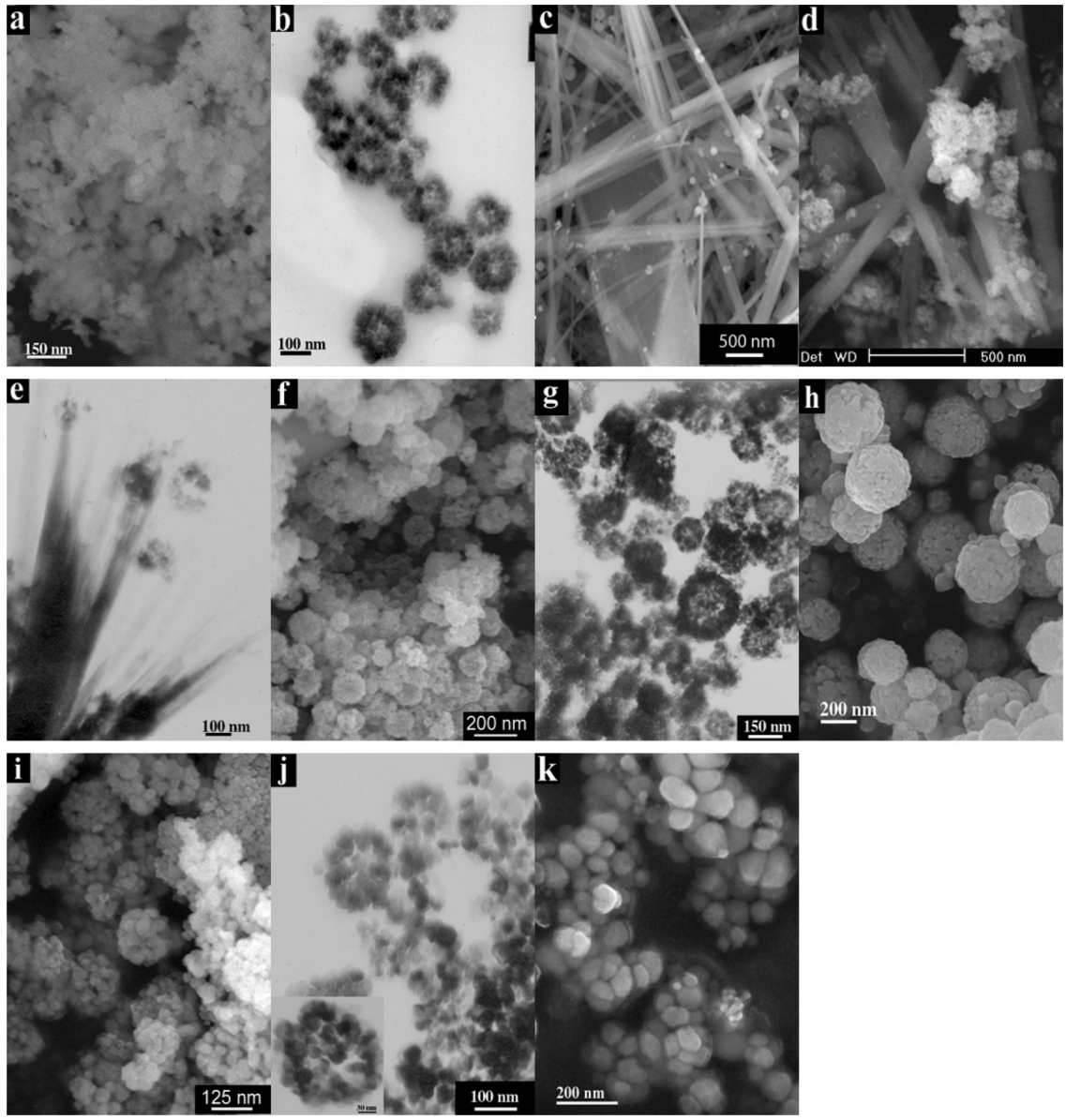

Figure 6. Influence of w with the solvothermal temperature being 180 °C. (a and b) SEM and TEM images of $w = 10$. (c) SEM image of $w = 20$. (d and e) SEM and TEM images of $w = 25$. (f and g) SEM and TEM images of $w = 30$. (h) TEM image of $w = 40$. (i and j) SEM and TEM images of $w = 50$. (k) SEM image for the absence of microemulsion.

brate every direction of the spheroid, and subsequent growth and Ostwald ripening occurred under solvothermal conditions, resulting in the formation of CoO submicrometer spheres.

In recent years, the nanostructure materials have shown great attraction for microwave absorbing and shielding material in the high-frequency range such as 1−20 GHz due to their many unique chemical and physical properties. Many reports focused on iron oxide, gallium-substituted ε-iron oxide, and cobalt phosphate micro/nanostructures.[14] However, the microwave absorption property of CoO nanostructures has not been studied so far. Thus, it is necessary to study the novel properties of these unique nanostructures and the intrinsic reasons for microwave absorption of the CoO nanostructures.

To reveal the microwave absorption properties of the typical samples, the reflection loss (RL) of CoO nanobelts and submicrometer spheres obtained at different conditions were calculated using the relative complex permeability and permittivity at a given frequency and thickness layer according to the transmit-line theory, which is summarized as the following equations: [13a,15]

$$Z_{in} = Z_0\sqrt{\mu_r/\varepsilon_r}\tanh[j(2\pi fd/c)\sqrt{\mu_r\varepsilon_r}] \quad (1)$$

$$\mathrm{RL\ (dB)} = 20\log|(Z_{in} - Z_0)/(Z_{in} + Z_0)| \quad (2)$$

where f is the microwave frequency, d is the thickness of the absorber, c is the velocity of light, Z_0 is the impedance of air and Z_{in} is the input impedance of the absorber. The relative complex permeability and permittivity were tested on a network analyzer in the range 2−18 GHz. The thickness of the sample is one of the crucial parameters which affect the intensity and the position of the frequency at the reflection loss minimum. Therefore, we prepared these samples with different thicknesses of 1.5, 2, 3, 4, and 5 mm in order to explore the influence resulting from the sample thickness. The results are shown in Figure 10. Figure 10a indicates that the microwave absorption performance of CoO nanostructures can be remarkably improved compared with that of the CoO bulk materials (12 times for nanobelts and 8 times for submicrometer spheres to bulk materials). As shown in Figure 10b, we can observe that CoO nanobelts obtained at $w = 20$ and $t = 12$ h have different

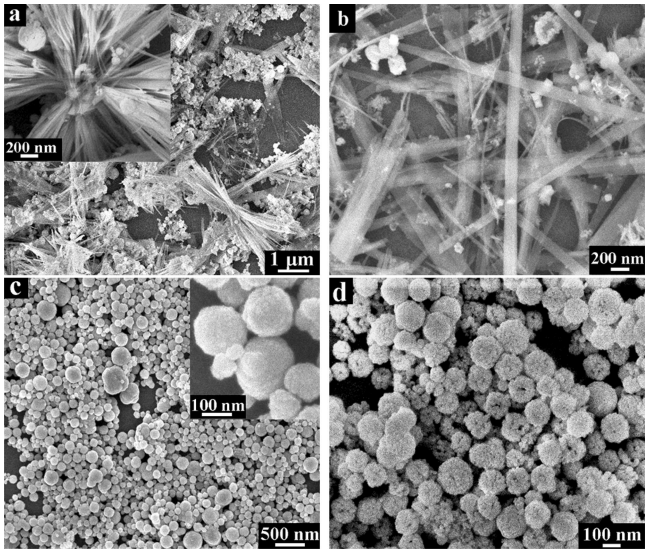

Figure 7. Influence of the solvothermal time (t) with the solvothermal temperature being 180 °C. (a) $t = 1$ h and (b) $t = 6$ h under the condition of $w = 20$. (c) $t = 1$ h and (d) $t = 6$ h under the condition of $w = 40$. The insets in (a) and (c) are the corresponding magnified SEM images.

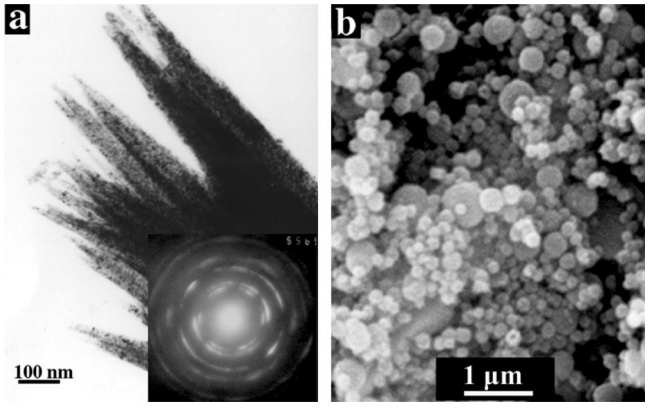

Figure 8. Electron microscopy characterization of the as-obtained samples at (a) $w = 20$, $T = 140$ °C and (b) $w = 40$, $T = 140$ °C. The inset of (a) is the typical SAED pattern taken on the nanobelt bundle.

microwave absorbance with the change of the sample thickness. With the increase of the sample thickness, all three samples reveal the absorbing peaks transfer to the low frequency. But for CoO nanobelts with a thickness of 3.0 mm, there are stronger wave absorbing broad peaks at 14.2 GHz in the frequency range of 4.0−18.0 GHz and the minimum reflection loss reaches −12.3 dB, while there is one broad wave absorbing peak at about 14.4 GHz in the frequency range of 8.0−17.0 GHz and the minimum reflection loss even reaches −8.7 dB for submicrometer spheres obtained at $w = 40$, $t = 1$ h with a thickness of 3.0 mm (see Figure 10c). For submicrometer spheres obtained at $w = 40$, $t = 12$ h with thickness of 4.0 mm, an absorbing peak at about 10.4 GHz in the frequency range of 4.0−18.0 GHz and a minimum reflection loss reaching −5.4 dB in the measuring frequency range were observed (see Figure 10d). Herein, the microwave-absorbing properties of CoO nanobelts obtained when $t = 12$ h is the best among the selected samples. Since CoO nanostrucures are antiferromagnetic materials, the variation of both the real and imaginary parts of the complex permeability are negligibly small, indicating almost no magnetic loss contribution from the three samples to the microwave absorption observed above. The main contribution to the

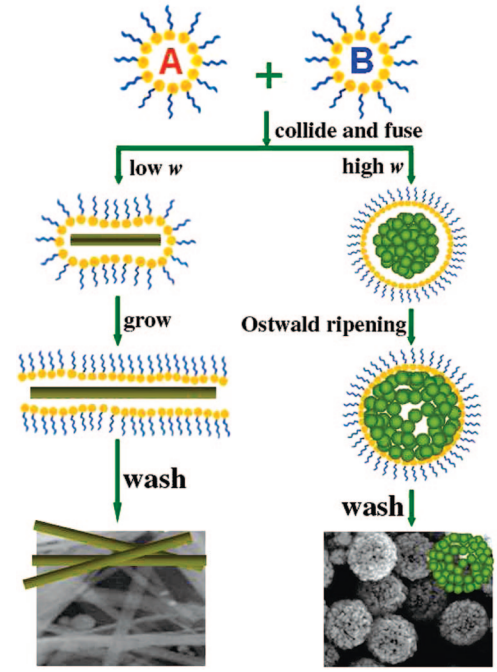

Figure 9. Schematic representation of the growth mechanism of CoO nanostructures by using the microemulsion as templates.

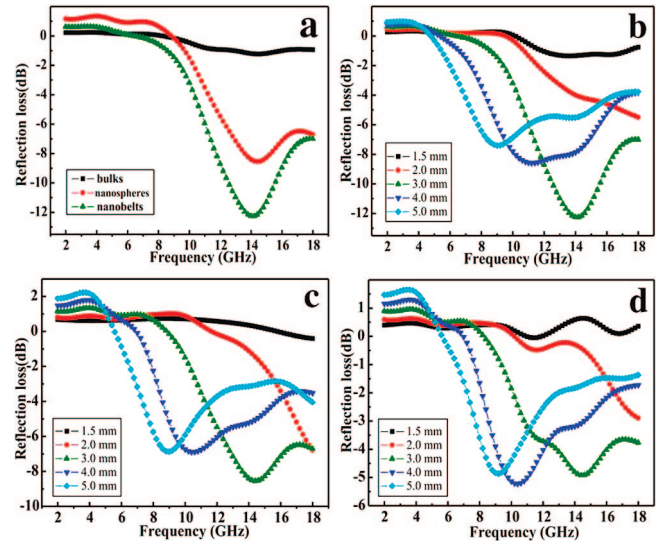

Figure 10. (a) Comparison of the microwave absorption performance for the CoO bulk materials and CoO nanospheres, CoO nanobelts. Microwave reflection loss of (b) CoO nanobelts obtained at $w = 20$, $t = 12$ h. (c) CoO nanospheres obtained at $w = 40$, $t = 1$ h. (d) CoO nanospheres obtained at $w = 40$, $t = 12$ h/paraffin wax composites versus frequency.

microwave absorption results is mainly from the dielectric loss rather than the magnetic loss. It is well-known that the permittivity mainly originated from electronic polarization, ion polarization, and intrinsic electric dipole polarization, on which the crystal structure, size, and shape of nanomaterials may have an improtant influence. On the basis of the electron microscopy characterization results, we can concluded that microwave absorbing properties are associated with the single crystal structure, the crystallization, and the aggregation degree of the nanocrystal building blocks. This also explains why the CoO nanostructures studied here have different microwave absorption properties.

Conclusions

In summary, stable CoO nanobelts and submicrometer spheres obtained by employing a quaternary microemulsion under solvothermal conditions have been prepared. The shape and size of CoO nanostuctures are well controlled by changing the value of the H_2O/CTAB molar ratio, the solvothermal time, and temperature. We are currently investigating the detail mechanism of the reductive reaction. The electromagnetism parameters reveal that the microwave absorption properties of CoO nanobelts were better than those of the submicrometer spheres, and both of them show a stronger microwave absorption performance than CoO bulk materials.

Acknowledgment. This work was supported by the Natural Science Foundation of China (NSFC, No. 20671011, 20731002, and 20801036). Professor B. Q. Wei is grateful for support from the 111 Project (NO. B07012) and G. B. Sun is grateful for support from the Analysis and Testing Fund of Beijing Normal University.

References and Notes

(1) (a) Zeng, H.; Li, J.; Liu, J.; Wang, Z.; Sun, S. *Nature (London)* **2002**, *420*, 395. (b) Pan, Z.; Dai, Z.; Wang, Z. *Science* **2001**, *291*, 1947. (c) Tarascon, J.; Armand, M. *Nature (London)* **2001**, *414*, 359. (d) Li, X.; Lou, T.; Sun, X.; Li, Y. *Inorg. Chem.* **2004**, *43*, 5442. (e) Yuan, J.; Laubernds, K.; Zhang, Q.; Suib, S. *J. Am. Chem. Soc.* **2003**, *125*, 4966. (f) Yang, H.; Zeng, H. *J. Phys. Chem. B* **2004**, *108*, 3492.

(2) (a) Sun, S.; Zeng, H.; Robinson, D.; Raoux, S.; Rice, P.; Wang, S.; Li, G. *J. Am. Chem. Soc.* **2004**, *126*, 273. (b) Skumryev, V.; Stoyanov, S.; Zhang, Y.; Hadjipanayis, G.; Givord, D.; Nogue's, J. *Nature (London)* **2003**, *423*, 850. (c) Lin, H.; Chiu, H.; Tsai, H.; Chien, S.; Wang, C. *Catal. Lett.* **2003**, *88*, 169. (d) Soriano, L.; Abbate, M.; Fernández, A.; González-Elipe, A.; Sirotti, F.; Sanz, J. *J. Phys. Chem. B* **1999**, *103*, 6676.

(3) (a) Yin, J.; Wang, Z. *J. Phys. Chem. B* **1997**, *101*, 8979. (b) Yin, Y.; Rioux, R.; Erdonmez, C.; Hughes, S.; Somorjai, G.; Alivisatos, A. *Science* **2004**, *304*, 711. (c) Park, J.; An, K.; Hwang, Y.; Park, J.; Noh, H.; Kim, J.; Park, J.; Hwang, N.; Hyeon, T. *Nat. Mater.* **2004**, *3*, 891. (d) Seo, W.; Shim, J.; Oh, S.; Lee, E.; Hur, N.; Park, J. *J. Am. Chem. Soc.* **2005**, *127*, 6188. (e) Ghosh, M.; Sampathkumaran, E.; Rao, C. *Chem. Mater.* **2005**, *17*, 2348. (f) Sun, X; Zhang, Y.-W.; Si, R.; Yan, C. *Small* **2005**, *1*, 1081. (g) Lagunas, A.; Payeras, A.; Jimeno, C.; Perics, M. *Chem.Commun.* **2006**, 1307.

(4) An, K.; Lee, N.; Park, J.; Kim, S.; Hwang, Y.; Park, J.; Kim, J.; Park, J.; Han, M.; Yu, J.; Hyeon, T. *J. Am. Chem. Soc.* **2006**, *128*, 9753.

(5) Narayanaswamy, A.; Xu, H.; Pradhan, N.; Peng, X. *Angew. Chem., Int. Ed.* **2006**, *45*, 5361.

(6) Zhang, W.; Han, M.; Jiang, Z.; Song, Y.; Xie, Z.; Xu, Z.; Zheng, L. *ChemPhysChem* **2007**, *8*, 2091.

(7) (a) Zhang, Y.; Zhong, X.; Zhu, J.; Feng, Y.; Song, X. *Nanotechnology* **2007**, *19*, 195605. (b) Zhang, Y.; Zhu, J.; Song, X.; Zhong, X. *J. Phys. Chem. C* **2008**, *112*, 5322.

(8) (a) Cao, M.; Hu, C.; Wang, E. *J. Am. Chem. Soc.* **2003**, *125*, 11196. (b) Sun, G.; Cao, M.; Wang, Y.; Hu, C.; Ren, L.; Huang, K. *Chem. Commun.* **2005**, 1740. (c) Cao, M.; Wu, X.; He, X.; Hu, C. *Chem. Commun.* **2005**, 2241. (d) Cao, M.; Wu, X.; He, X.; Hu, C. *Langmuir* **2005**, *21*, 6093.

(9) Kruger, G.; Reynhardt, E. *Acta Crystallogr. Sect. B* **1978**, *34*, 915.

(10) (a) Schmidt, K.; Muller, A. *Coord. Chem. Rev.* **1976**, *19*, 41. (b) Guo, L.; Liu, C.; Wang, R.; Xu, H.; Wu, Z.; Yang, S. *J. Am. Chem. Soc.* **2004**, *126*, 4530.

(11) Wang, L.; Vu, K.; Navrotsky, A.; Stevens, R.; Woodfield, B.; Boerio-Goates, J. *Chem. Mater.* **2004**, *16*, 5394.

(12) (a) McIntyre, N.; Cook, M. *Anal. Chem.* **1975**, *47*, 2208. (b) Tan, B.; Klabunde, K.; Sherwood, P. *J. Am. Chem. Soc.* **1991**, *113*, 855.

(13) Clark, S.; Fletcher, P. D. I.; Ye, X. L. *Langmuir* **1990**, *6*, 1301.

(14) (a) Han, X.; Wang, Y. *Phys. Scr.* **2007**, *T129*, 335. (b) Ohkoshi, S.; Kuroki, S.; Sakurai, S.; Matsumoto, K.; Sato, K.; Sasaki, S. *Angew. Chem., Int. Ed.* **2007**, *46*, 8392. (c) Wen, H.; Cao, M.; Sun, G.; Xu, W.; Wang, D.; Zhang, X.; Hu, C. *J. Phys. Chem. C* **2008**, *112*, 15948.

(15) (a) Matsumoto, M.; Miyata, Y. *IEEE Trans. Magn.* **1997**, *33*, 4459. (b) Singh, P.; Babbar, V.; Razdan, A.; Puri, R.; Goel, T. *J. Appl. Phys.* **2000**, *87*, 4362. (c) Maeda, T.; Sugimoto, S.; Kagotani, T. *J. Magn. Magn. Mater.* **2004**, *284*, 113.

JP8092447